LEGIBILITY NOTICE

A major purpose of the Technical Information Center is to provide the broadest dissemination possible of information contained in DOE's Research and Development Reports to business, industry, the academic community, and federal, state and local governments.

Although portions of this report are not reproducible, it is being made available in microfiche to facilitate the availability of those parts of the document which are legible.

3

CONF-8910240--

LA-UR--89-3123

DE90 001828

Los Alamos National Laboratory is operated by the University of California for the United States Department of Energy under contract W-7405-ENG-36

TITLE: STRENGTHENING MECHANISMS OF TUNGSTEN POWDER REINFORCED URANIUM

AUTHOR(S): Melissa Ann Krawlzcki Lewis
Mary Ann Hill
Anthony D. Rollett
Andreas Mortensen

SUBMITTED TO: TMS/ASM Fall Meeting, Proceedings, Indianapolis
October 1-5, 1989

Los Alamos Los Alamos National Laboratory
Los Alamos, New Mexico 87545

STRENGTHENING MECHANISMS IN TUNGSTEN POWDER REINFORCED URANIUM

Melissa A. K. Lewis, Mary Ann Hill, Anthony D. Rollett, and Andreas Mortensen*

Los Alamos National Laboratory
P. O. Box 1663
Los Alamos, New Mexico 87501

* Massachusetts Institute of Technology
Room 8-401
Cambridge, Massachusetts 02139

Abstract

Tungsten powder reinforced uranium exhibits a three-fold increase in yield strength due to precipitation hardening. The tungsten-rich interphase precipitates form at moving phase boundaries during slow cooling. Further increases in yield strength, attained with increasing tungsten content, are due to composite strengthening; this is verified by increasing elastic modulus with increasing tungsten content. Age hardening behavior is observed, with strengthening occurring at aging temperatures low in the alpha phase. Aging higher in alpha gives initial strengthening followed by rapid overaging. Beta phase aging results in a very soft structure with precipitates visible optically. Wrought material exhibits significant strain hardening as well as composite strengthening due to elongation of the tungsten particles.

Introduction

The search for high strength, high density alloys retaining some measure of ductility has been in progress for close to forty years. Many materials used to date require precise heat treating and/or working schedules to achieve the properties necessary for high strength, high density applications. The uranium-tungsten system exhibits significant as-cast strength, and shows promise of increased strength, as well as increased ductility, with thermo-mechanical treatment. The strengthening mechanisms responsible for the mechanical behavior of the uranium-tungsten system are under investigation; an increased understanding of the mechanisms at work in the material will lead to the development of processing and/or alloy additions that balance high strength with reasonable ductility.

The suspected strengthening mechanism is precipitation hardening, since this is observed in many other uranium binary systems.[1][2][1] In particular, interphase precipitates, such as those found in alloy steels containing strong carbide formers as alloy additions, are suspected.[3] Interphase precipitates have been identified in many uranium alloys as a "pearlitic" decomposition of the beta phase. Unlike conventional pearlitic reactions, the growth of the structure is controlled by interface movement and not diffusion.[4][5] This study includes a search for evidence of interphase precipitates, future studies will examine reaction kinetics.

Materials and Procedures

The depleted uranium used in this study was purchased as plate feed stock from Y-12. The pure tungsten powder was purchased from General Electric, while the impure powders were supplied by Kennametal. Impurity levels in each of the powders are listed in Table I. The target compositions of tungsten in uranium used in the study were 2 vol%, 10 vol%, 20 vol%, 25 vol%, and 30 vol%. Tungsten levels were determined by x-ray fluorescence, carbon levels by mass spectroscopy, and other elements by solution spectroscopic analysis.

Material used in this study was cast in the MST-6 foundry at Los Alamos National Laboratory. A in-depth study, led by Paul Dunn of Los Alamos, detailed casting conditions necessary for production of castings with a homogeneous distribution of tungsten. The material was cast in vacuum induction furnaces. Depleted uranium feed stock and tungsten powder were layered in a graphite crucible spray-coated with zirconia or yttria, melted and superheated approximately 200 degrees Celsius. The melt was allowed to outgas, and then was bottom-poured into coated graphite molds. The power to the furnace coil was then turned off, and the casting cooled overnight under vacuum.

---

1 These two papers provide an overview of uranium alloy transformations and strengthening mechanisms. They also provide references to scores of specific alloy systems.

Table I: Compositions of Starting Materials (ppm)

	Depleted Uranium	W-204 impure	W-211 impure	W-191 impure	W-234 impure	W234-2 impure	W-178 pure
Carbon	<30					100	
Nickel	11	500	500	100-1000	850	1000	<10
Iron	26	4000	6000	100-1000	1900	2000	30
Copper	22	8	10	100-1000	225	100	<1
Moly	<10	40	<40	0.1%-1%		120	500
Cobalt	1	100	200	10-100		<10	<10
Chromium	2	20	13	10-100		<10	<10
Titanium	9	80	40	100-1000		25	<30
Calcium	<10	40	25	10-100		20	<3
Silicon	15	1-10	1-6	10-100		<100	10
Aluminum	9	7	6	10-100		<10	<10
Magnesium	3	2	1.3	<10		<10	<1
Niobium	10	<130	<130	10-100		<10	<300
Manganese	8	2.5	4	<10		<10	<3

Porosity was discovered in a number of castings, presumably from gases trapped in clumped powders, or de-gassing of the tungsten powders. A hot isostatic press cycle was developed to heal this porosity. Once again the castings were placed in a coated graphite pan, and were heated to 1000° Celsius at a pressure of nearly 207 MPa (30,000 psi).

A casting of tungten in copper was produced for comparison. Tunsten and copper are mutually insoluble, so the microstructure was intended to show distribution of the original tungsten powder morphology. Only one attempt was made at casting, and the distribution of tungsten, as a result, was poor.

Plate material for the rolling study was cast in the manner described above. After casting, the material was hot-rolled at a temperature of 625 °C in a salt bath composed of potassium-lithium carbonate salt. The plate was reduced from a thickness of 25.4 mm (1") to 2.3mm (0.090"). A vacuum anneal at 650 °C for two hours was then performed. The samples were warm-rolled at 325 °C to a nominal percent reduction through a combination of reduction and intermediate annealing steps. The reductions produced through this process were 12%, 21%, 30%, and 69%. Tensile samples were cut from each sheet.

The material selected for the heat treating study was uranium-2wt% tungsten. According to the binary phase diagram, this amount of tungste should be completely solutionized in the melt. The aim was to observe the effects of possible solution or precipitation strengthening without the interference of composite strengthening acheived at higher tungsten loadings. The material was cast as rod stock, and sliced into disks approximately 5 mm (0.2") thick. These disks were solutionized in the gamma phase at 1070 °C for 18.5 hours and quenched in room temperature agitated oil.

Results and Discussion

Optical Microscopy and Image Analysis

A comparison of the tungsten powder in the uranium matrix and the tungsten in a copper matrix reveals the dissolution of tungsten in uranium. Figure 1 is a micrograph which shows the particle size and shape distribution of tungsten in a copper matrix. Tungsten is insoluble in copper, so this is a fairly accurate representation of the starting powder morphology, . In contrast, Figure 2 shows that the tungsten size and shape distribution in the uranium matrix is significantly altered from the original powder morphology. The tungsten in the as-cast matrix has lost its acicular character, and appears to have broken up along the grain boundaries within the powder particles. The powder used in the castings above contained a high level of impurities (W204, W211, W191, and W234 from Table I).

The material in Figure 3 is the uranium-tungsten composite produced with a high purity tungsten powder (W178 from Table I). This micrograph indicates the tungsten powder particles do not break up to the extent seen in the impure powder. The acicular particles present in the original powder are not present in the as-cast structure.

It is apparent from the above data, that some amount of tungsten goes into solution in uranium during the casting procedure. This is determined by the disappearance of the acicular powder particles (approximately ten percent of the powder). It is also apparent that the presence of impurities in the tungsten aids in the break-up of the particles; the impurites may also increase the amount or rate of tungsten going into solution in the uranium matrix.

Figure 4 is a plot of the image analysis results for size distribution. The end bars for each material are at the 5th and 95th percentile. The ends of the boxes are the 25th and 75th percentile, and the thick line is the mean of the distribution for each material. The as-cast impure tungsten in uranium exhibits a much smaller range of particle sizes, as well as a significantly lower mean size than the starting powder. This indicates a break up of the powder particles in the melt, and/or dissolution and precipitation of tungsten. The distribution of sizes in the copper casting made with impure powder and the uranium casting with pure powder are essentially the same as the original powder, except for the tendency toward agglomeration in the melt. This agglomeration leads to a slightly larger range of sizes, as well as a larger mean particle size.

Figure 1: Impure Tungsten Powder in a Copper Matrix

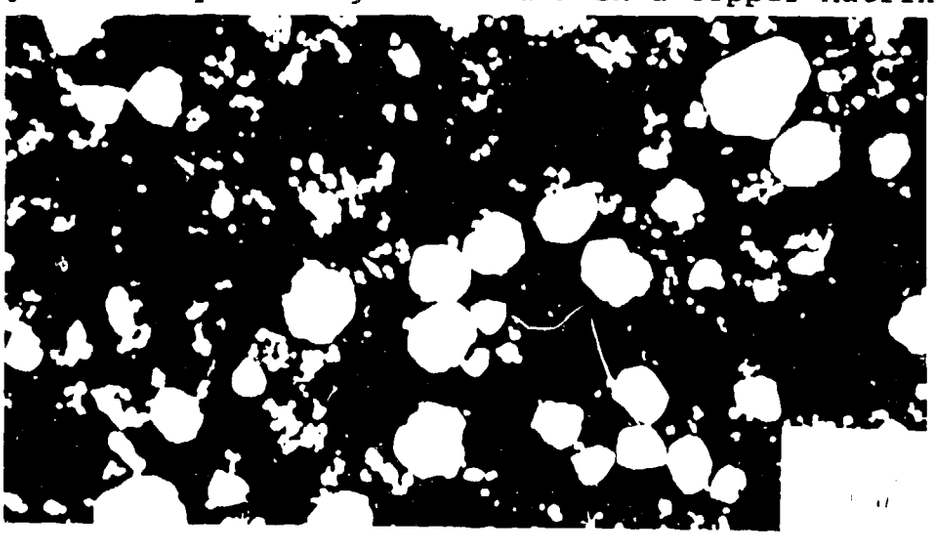

Figure 2: Impure Tungsten Powder in a Uranium Matrix

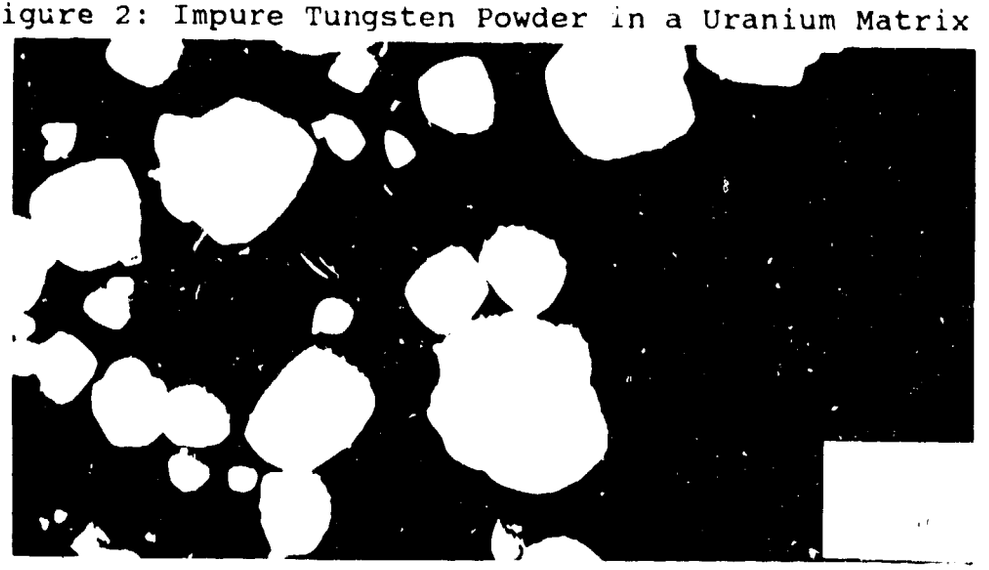

Figure 3: Pure Tungsten Powder in a Uranium Matrix

Figure 5 is a plot of particle irregularity as determined through image analysis. The measure of irregularity is the Formfactor whose value is determined by equation 1, where A is the area of the particle and P is its perimeter. The maximum formfactor value is 1, which represents the most regular shape - a circle. At the top of the plot are sample shapes corresponding to particular formfactor values.

$$Formfactor = \frac{4\pi A}{P^2} \qquad (1)$$

The distribution of particles in the copper casting is again essentially that of the original powder, with the exception of a slightly higher irregularity caused by agglomeration. The distributions in the uranium castings produced with impure tungsten powder show an increase in particle regularity over the starting powder. The acicular particles and sharp edges are dissolved as thermodynamics suggest. The two percent impure tungsten in uranium has the highest regularity, since most or all of the tungten is in solution at the hold temperature in the casting procedure. The tungsten that precipitates out of solution is essentially spherical. The pure tungsten powder in the uranium matrix is slightly more regular than the starting powder, suggesting dissolution of acicular particles and sharp edges, but not break up or precipitation to the extent found with the impure tungsten.

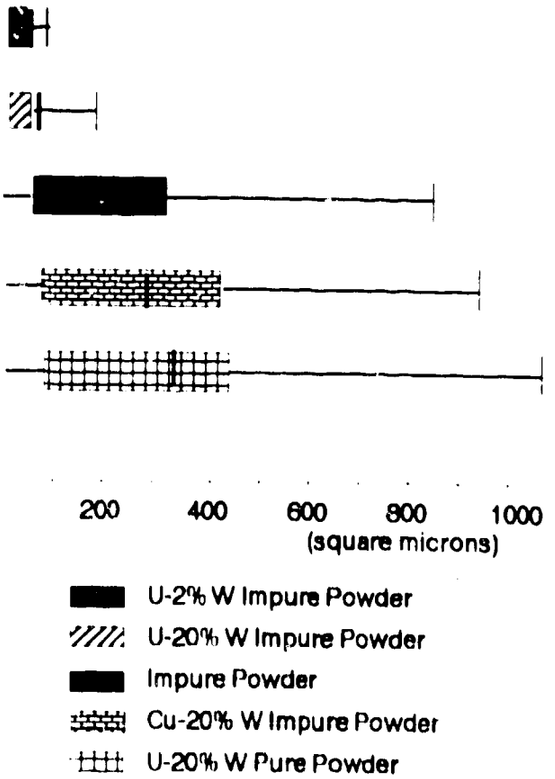

Figure 4: Particle Size Distribution

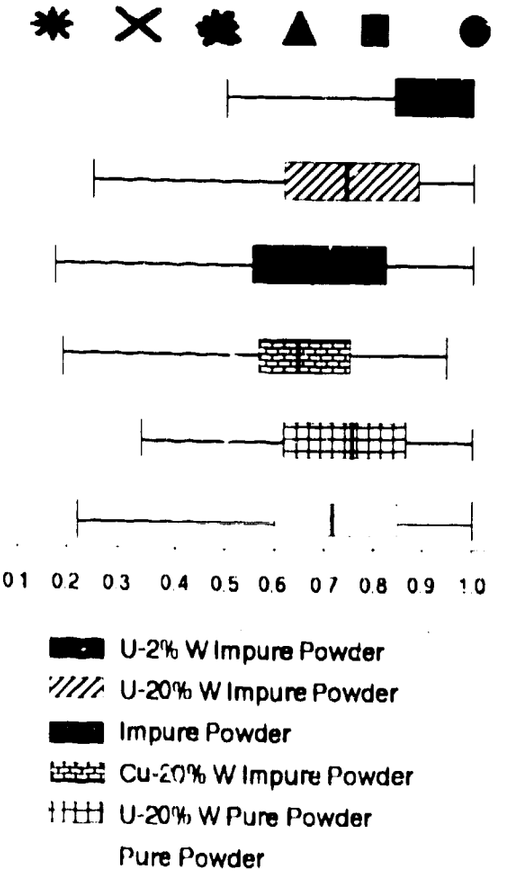

Figure 5: Particle Shape Distribution -- Formfactor

The wrought material used in this study is pictured in Figure 6. This particular sample was rolled to a 69% reduction, and annealled. The micrograph shows that some of the tungsten particles have been extensively elongated, while others are only slightly deformed.

The material used in the age hardening study was also examined optically, the results and discussion appear in the section on heat treating.

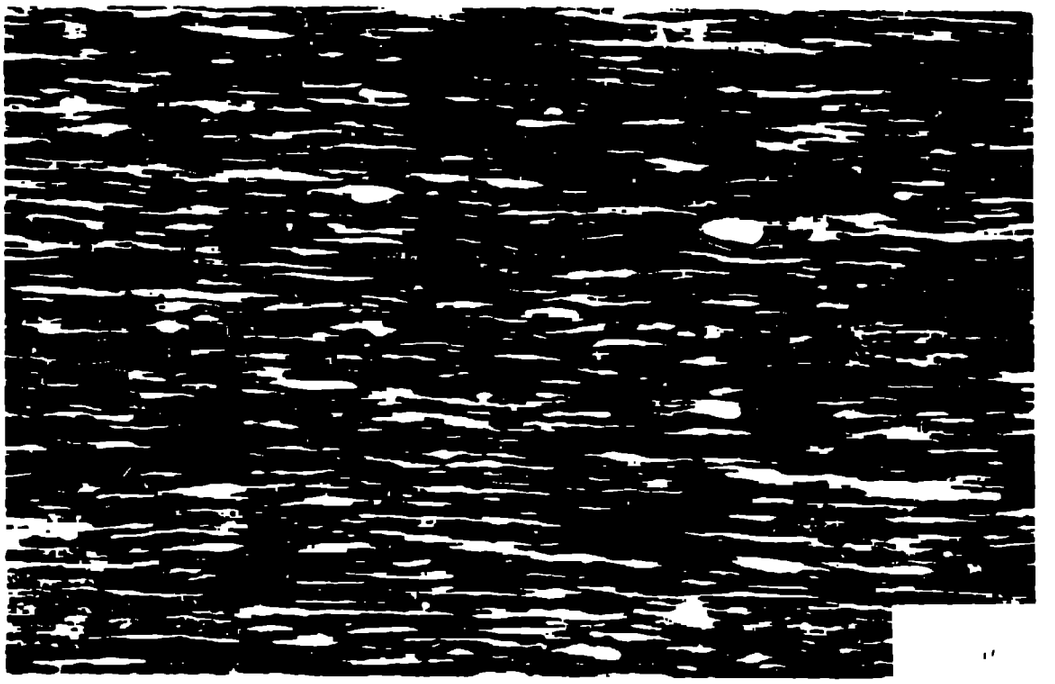

Figure 6: Uranium -20% Tungsten Rolled to 69% Reduction and Annealled

Transmission Electron Microscopy

Transmission electron microscopy of the uranium matrix containing 20% impure tungsten powder revealed precipitates approximately 5 to 10 nanometers in diameter, aligned in roughly parallel rows. Figure 7 is a photograph of this material taken at 50,000x. The precipitates are not observed in all grains, and problems in making foils with large thin areas makes it difficult to predict the extent to which they actually occur. A foil of the same material was aged for one hour at 600 ^{o}C to document the change in precipitates. Figure 8 shows a randomization of location and precipitate coarsening as a result of aging.

Material composed of 2% impure tungsten in uranium was observed in the TEM in two conditions. Figure 9 is the structure in the as-cast condition, having been slow-cooled from the melt. The precipitates are aligned, but they are larger and the row spacing is greater than was observed in the 20% tungsten material. Lack of thin area prevented further study of this sample. The second condition is material that was solutionized in the gamma phase and quenched. Figure 10 is this structure, showing few precipitates with a random orientation.

Evidence from both optical and electron microscopy combined with binary phase information indicates that nucleation and growth of precipitates occurs by interphase precipitation in the uranium-tungsten composite system. The precipitates form during an allotropic phase transformation, due to a decrease in tungsten solubility. The second phase precipitates on the moving phase boundary resulting in rows of precipitates with a discontinuous lamellar character. As was mentioned earlier, similar interphase precipitation is documented for vanadium, titanium, and niobium steels, as well as dilute uranium alloys.

Analyses: X-ray, and STEM

X-ray analysis of as-cast and solutionized and quenched uranium-tungsten show that the matrix is composed solely of alpha uranium. As predicted by the low solubility of tungsten in uranium, neither gamma nor beta uranium was retained at room temperature, even in the quenched structure.

Spectral analysis performed with a STEM attachment on the TEM determined the matrix composition as uranium. The spectra of precipitates in the as-cast and quenched structures both include large tungsten peaks and small uranium peaks, with no other elements detected, as seen in Figure 11 (a) and (b). The uranium peaks are likely a result of matrix material analyzed with the precipitate, since no intermetallics have been reported in this system. It is concluded that the second phase is tungsten-rich, the only other possible constituent detectable in the STEM being uranium.

Figure 7: As Cast Uranium - 20% Tungsten

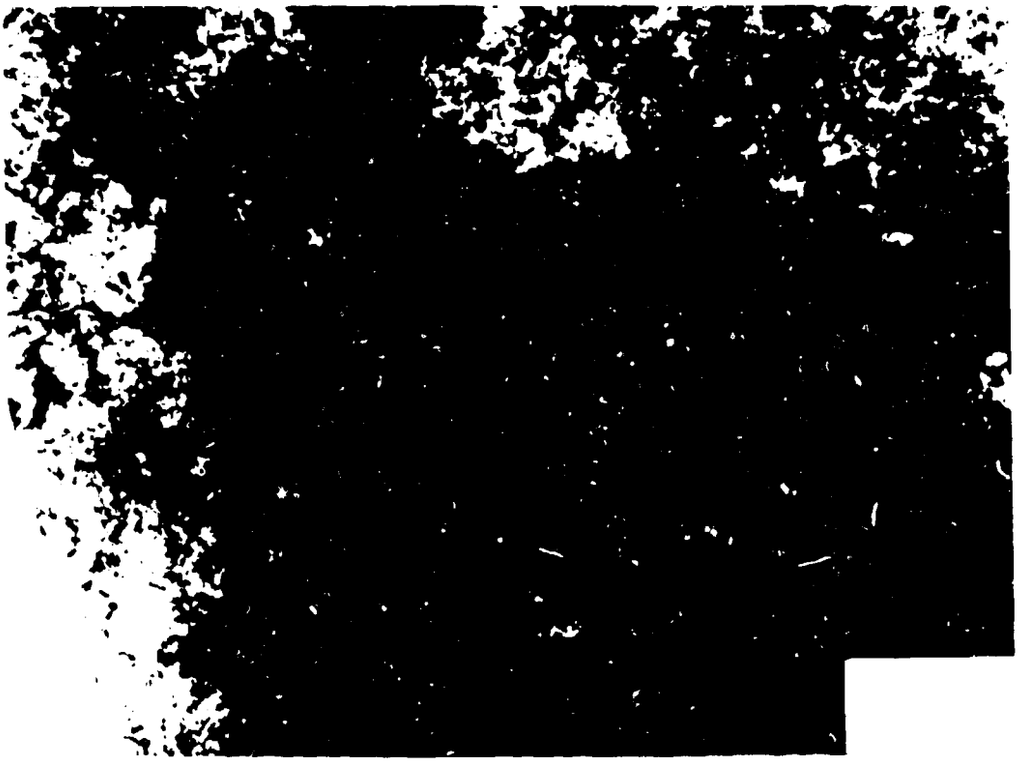

Figure 8: Uranium - 20% Tungsten Aged at 600 °C for 1 Hour

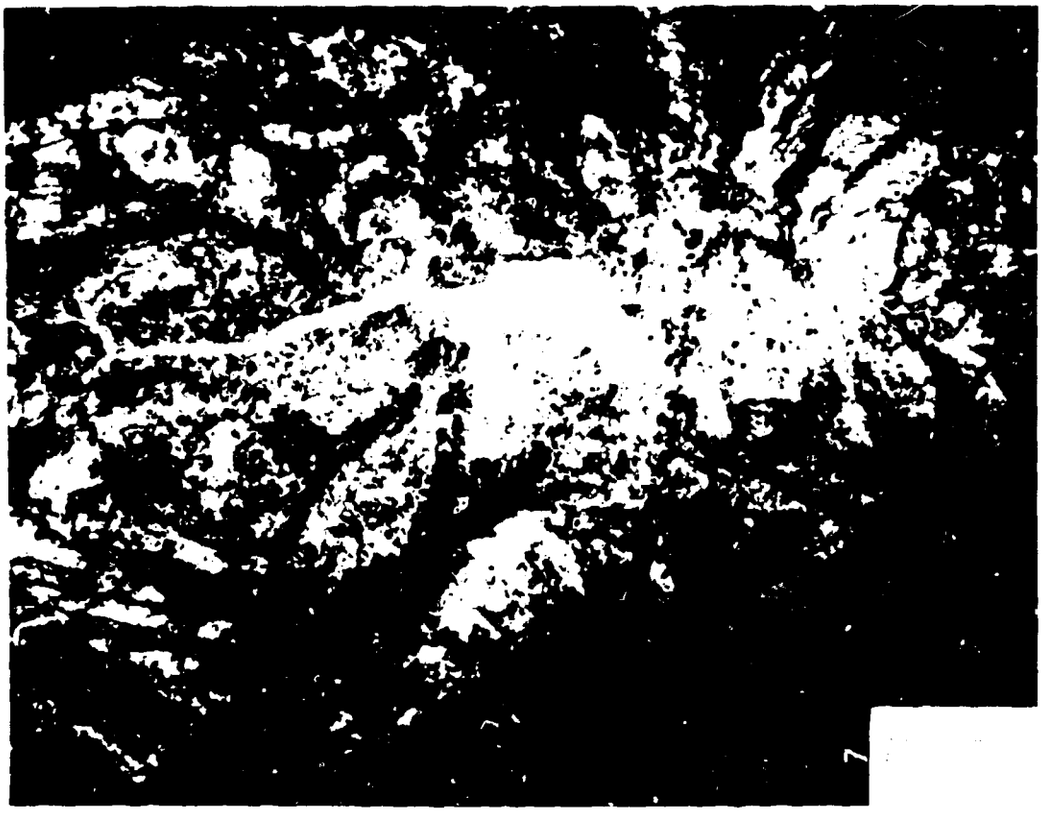

Figure 9: Uranium - 2% Tungsten As Cast

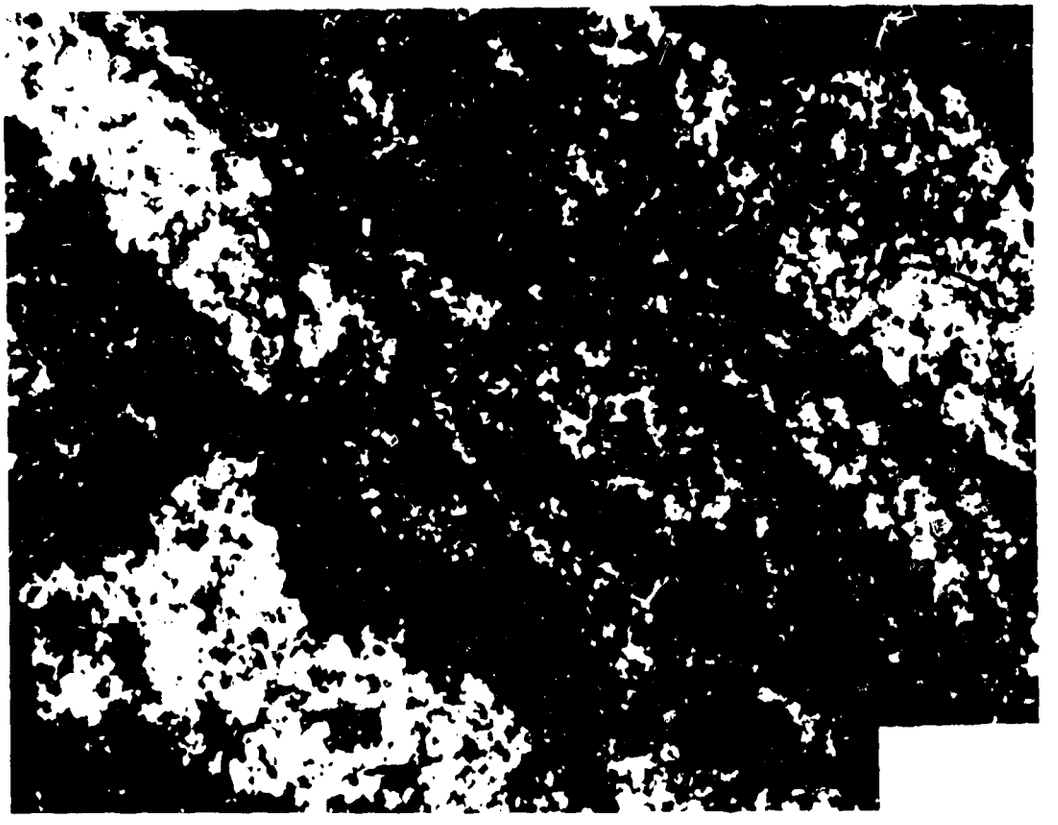

Figure 10:Uranium - 2% Tungsten Solutionized and Quenched

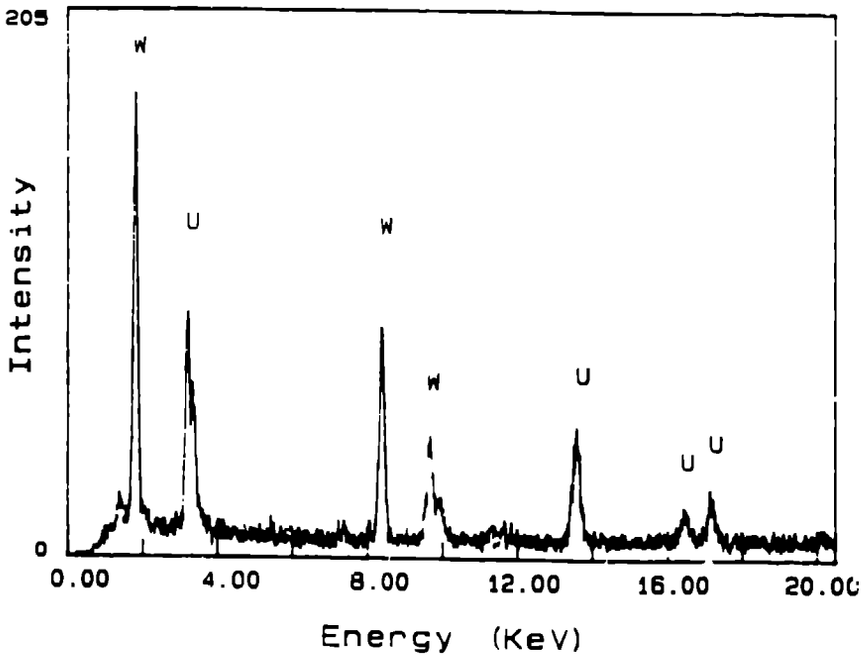

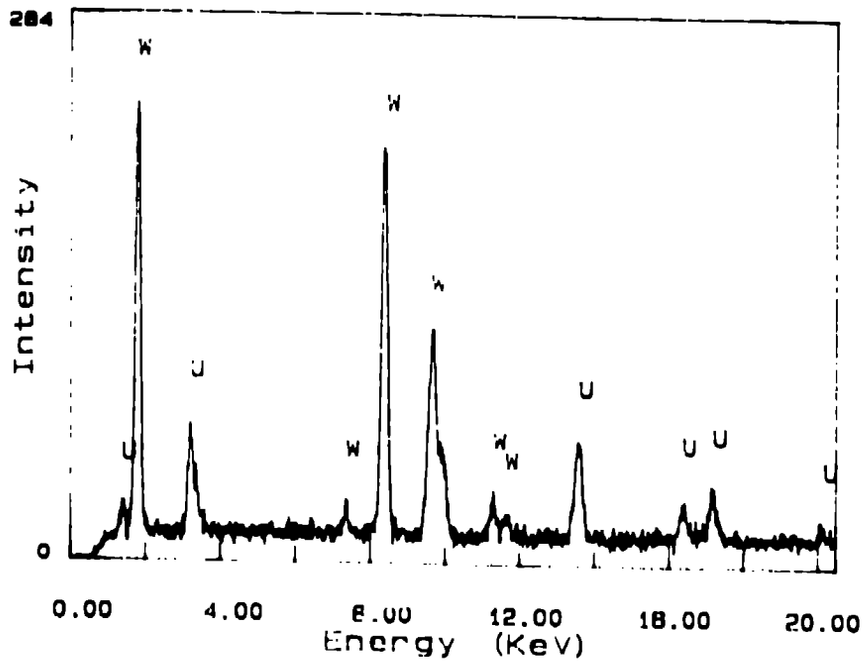

Figure 11: (a) (Top) STEM Spectrum of As Cast Precipitate
(b) (Bottom) STEM Spectrum of Quenched Precipitate

Heat Treating

Uranium with two percent tungsten added shows a definite age hardening response. Figure 12 is a graph of Rockwell C Hardness versus time at aging temperature for material which has been gamma solutionized and quenched. Aging temperatures low in the alpha region produce a gradual increase in hardness. Temperatures intermediate in alpha exhibit a more rapid increase in hardness with time at temperature. Aging high in alpha results in rapid overaging. The beta phase age with slow cool through the beta to alpha transition results in an extremely soft structure with precipitates in the discontinuous lamellar structure visible optically. Figure 13 is the microstructure of the sample aged in the beta phase and air cooled. Precipitation hardening is the mechanism suspected, although this has not yet been confirmed through electron microscopy. A more thorough study of the aging curves is in progress, including investigation of tensile properties.

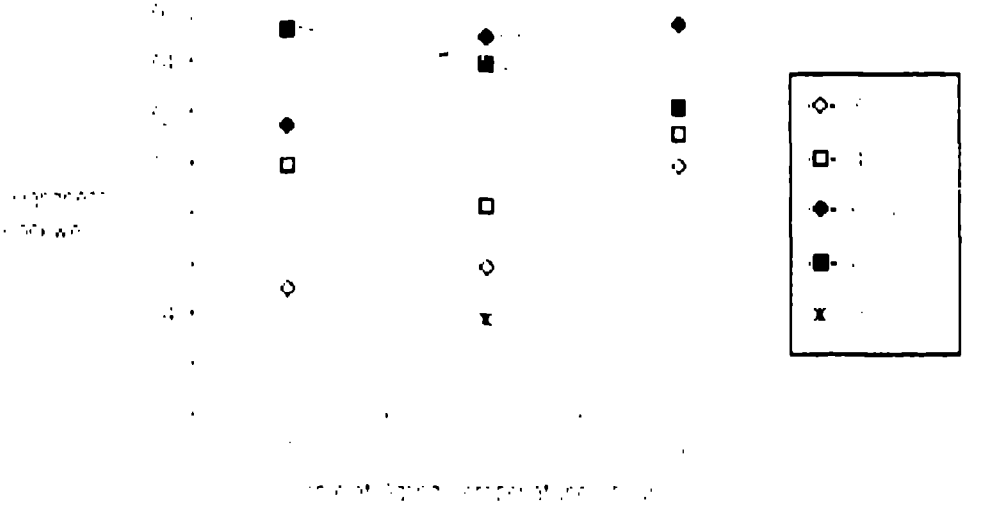

Figure 12: Results of Age Hardening Study
Hardness: Rockwell C

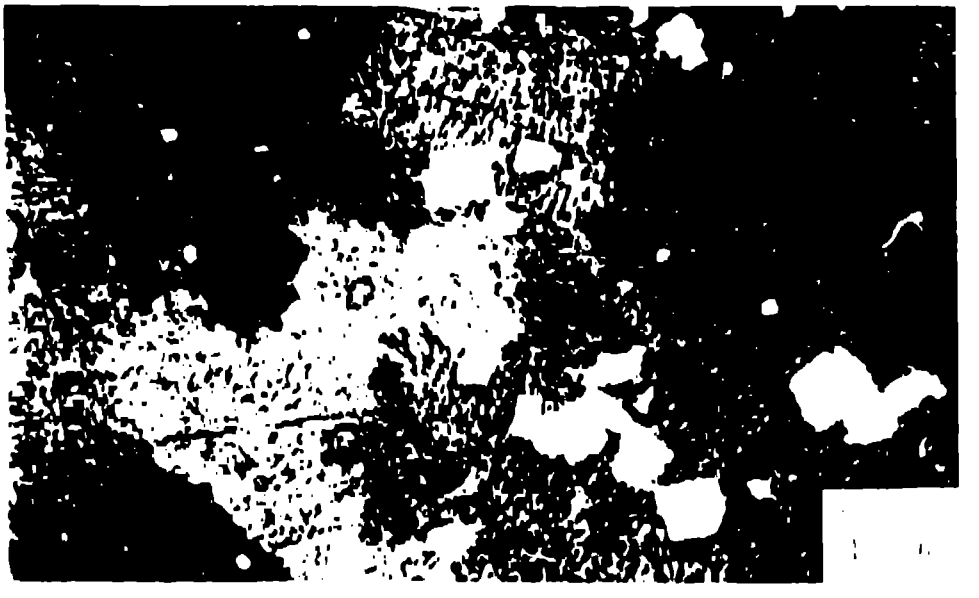

Figure 13: Aligned Precipitates in Beta Aged Uranium-Tungsten

Mechanical Testing

Much of the initial data collected on the uranium-tungsten material was four point bend data. Bend tests of samples with a round cross section were chosen due to constraints imposed by the original material design, which included monolithic tungsten reinforcements. It was deemed to be the only valid method of testing the composite in that configuration. Recent numerical analysis indicates that the geometry of the round cross section causes the yield strength to be overestimated by as much as twenty percent.[6] The properties listed in Table 2 are self-consistent, but should not be compared to other values found in the literature, unless those values were also determined through flexure of round rods. An effort is underway to collect tensile data on the majority of these materials so direct comparisons to uranium alloy literature may be made. Table 3 contains the tensile data obtained to date.

The flexure data of Table 2 is plotted in Figure 14, as yield strength versus tungsten content. The initial jump in strength is attributed to formation of interphase precipitates. Presumably the contribution of precipitation hardening is constant once the solubility limit of the matrix has been reached. The gradual increase in strength associated with increase in tungsten content is believed to be caused by composite strengthening effects analagous to those observed in particulate reinforced materials. The increase in Young's Modulus with greater additions of tungsten confirm that composite strengthening is active in this system.

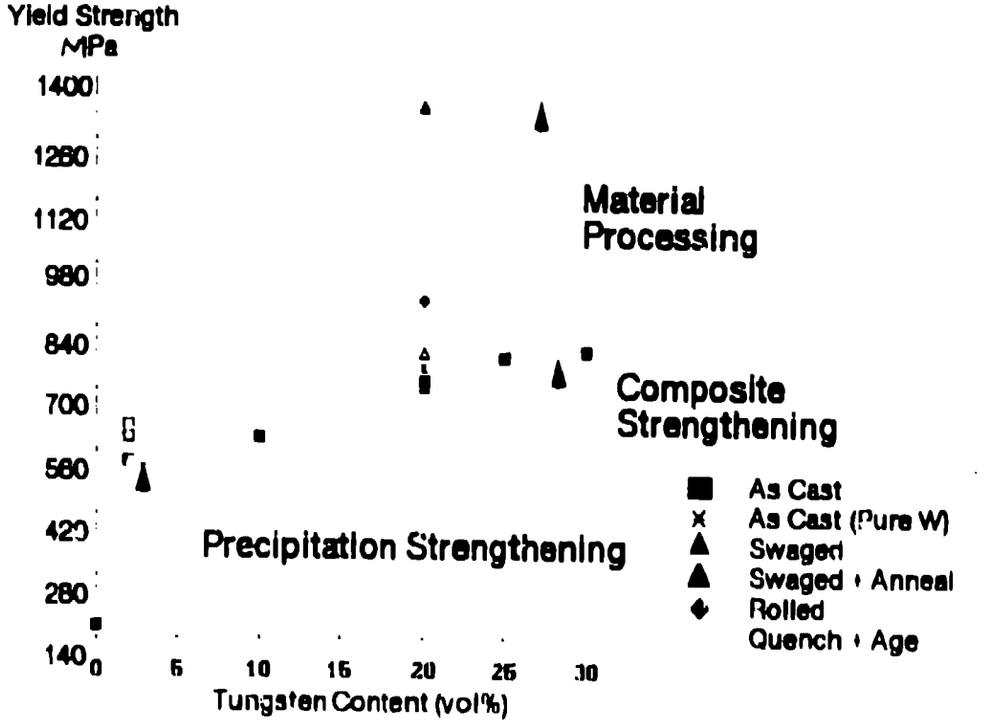

Figure 14: Yield Strength as a Function of Tungsten Content and Processing

TABLE 2 Mechanical Properties of Uranium-Tungsten Alloys in Flexure

Casting #	Tungsten wt% top/bot	Yield Strength MPa/(ksi)	Young's Modulus GPA/(Msi)
86k-16	none	165.8/24.05	148.2/21.5
87x-115/6	1.5	530.6/76.95	155.1/22.5
86x-58	10	586.1/85	-
86x-36	20	679.8/101.2	188.9/27.4
88c-327	20	709.7/102.93	195.1/28.3
88x-146 (plate)	20	947.7/137.45	209.5/30.39
87x-118 (pure)	20	737.8/107	170.7/24.75
swaged	20	1316.9/191	192.7/27.95
swaged + anneal	20	772.2/112	183.4/26.6
86k-47	25	761.7/110.47	194.4/28.19
86x-59	30	775.7/112.5	202.7/29.4

TABLE 3 Mechanical Behavior Of Uranium-Tungsten Alloys in Tension (As Cast)

Casting	Actual W wt% top/bot	Yield Strength MPa (ksi)	Young's Modulus GPa (Msi)	Elong. (%)	Reduct. in Area (%)	UTS MPa (ksi)
88x-115/6	1.53/ 1.42	328.3 (47.6)	171.4 (24.9)	6.6	10.4	702.6 (101.9)
88c-327		446.5 (64.8)	201.9 (29.3)	1.91	1.65	705.2 (102.3)
87x-118		415.1 (60.2)	196 (28.4)	1.75	3.06	672.3 (97.5)

The effect of precipitation hardening on yield strength can be simply estimated using the Orowan stress for moving dislocations past obstacles. Equation 2 can be used to calculate the resolved shear stress (τ) if the shear modulus (G), Burger's vector (b), and particle spacing (λ) are known.

$$\tau = \frac{Gb}{\lambda} \qquad (2)$$

The particle density was estimated from Figure 7. This value was inverted, and the cube root calculated to give an effective particle spacing of 49 nanometers (1.93E-6 inches). An average shear modulus of 48.3 GPa (7 Msi) was assumed, and the Burger's vector used was the lattice parameter of the shortest axis, 2.85 Angstroms (1.1E-8 inches). The resulting shear stress, approximately one-third the yield stress, is 317.9 MPa (46.1 ksi). The predicted strength due to precipitation hardening is then 953.6 MPa (138.3 ksi). This is slightly less than double the observed increase attributed to precipitation. As was explained earlier, not all grains contain precipitates. The small sampling area thus may have led to an overestimation of the yield strength. It is concluded that precipitation strengthening can account for the observed increase in yield strength.

The Young's Modulus of the composite (E bar) as a function of tungsten content shows a definite increase with increasing tungsten content. Figure 15 is a plot of the moduli determined experimentally in flexure with upper and lower bounds calculated using the Tsai-Halpin Model.[7] This model was formulated for whisker reinforced composites and is purely empirical, but has been found to predict the modulus of particulate composites. Equation 3 is the formula for determining the longitudinal modulus, and equation 4 the transverse modulus. E_M is the modulus of the matrix, L is the whisker length, D_W the diameter of the whisker, and V_f is the volume fraction of whiskers. Equation 5 is the definition of variabl "a", which is 1 for a roughly spherical particle. Equation 6 is the composite modulus; when the L/D ratio is 1, the longitudinal and transverse moduli are equal, resulting in equation 7. The bounds were calculated using the upper and lower values obtained for the moduli of pure tungsten and uranium in flexure.

$$E_l = E_M \frac{(1 + ab V_f)}{(1 + 2b V_f)} \tag{3}$$

$$E_t = E_M \frac{(1 + 2b V_f)}{(1 - b V_f)} \tag{4}$$

$$a = \frac{2L}{D_W} \tag{5}$$

$$b = \left(\frac{E_W / E_M - 1}{E_W / E_M + a}\right)$$

$$E = \frac{3}{8} E_l + \frac{5}{8} E_t \tag{6}$$

$$E = \frac{(1 + 2b V_f)}{(1 - b V_f)} \tag{7}$$

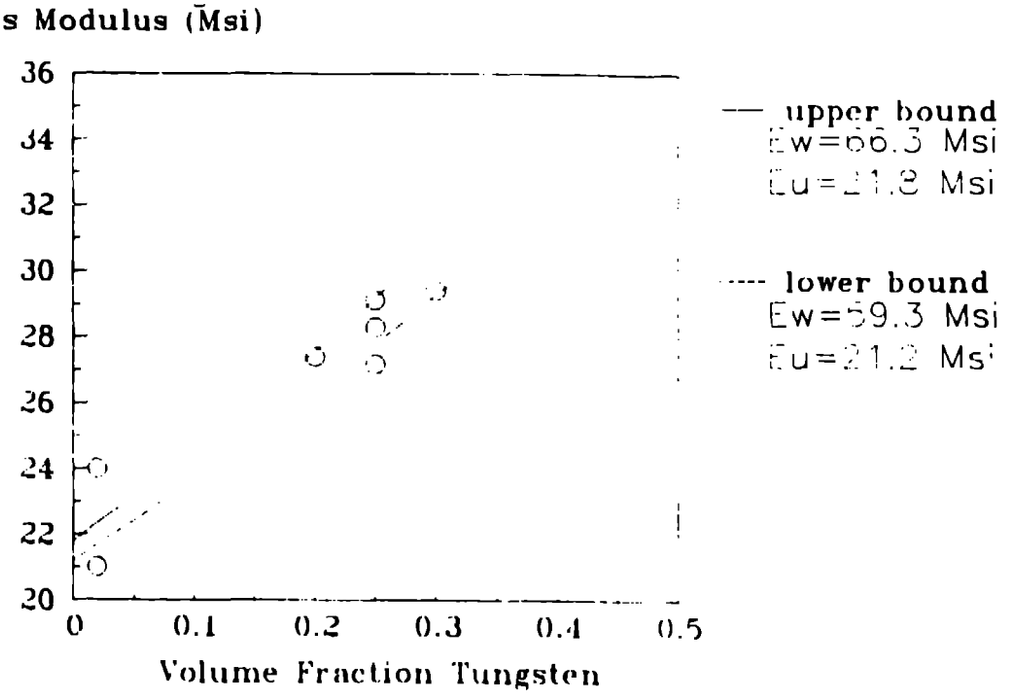

Figure 15: Tsai-Halpin Model for Composite Modulus Tungsten Reinforced Uranium

Properties of the wrought material are contained in Table 4. The yield and ultimate tensile strengths increase dramatically as the amount of work in the material is increased. This is expected of uranium, which strain hardens easily. The modulus increases to a peak value of 241 GPa (35 Msi) at 21% cold work, and decreases slightly after that. The increase in modulus occurs as the tungsten particles elongate during working. The decrease with further working indicates possible fracturing of the tungsten strings. Optical microscopy will be performed to verify this. As expected, the ductility in the material decreases with increasing work. Annealling after rolling significantly lowers the strength levels, but the ductility is improved by a factor of two.

TABLE 4 Mechanical Behavior of Wrought U-20%W in Tension

Warm Work (%)	Yield Strength MPa (ksi)	Young's Modulus GPa (Msi)	Elong. (%)	Reduct. in Area (%)	UTS MPa (ksi)
12	727.4 (105.5)	196.5 (28.5)	5.85	10.15	1131.8 (164.2)
21	766.7 (111.2)	241.3 (35)	5.75	11.55	1188.35 (172.4)
30	784 (113.7)	225.5 (32.7)	4.75	6.45	1245.9 (180.7)
69	887.4 (128.7)	199.3 (28.9)	1.5	4.55	1423.5 (206.5)
69 + anneal	673 (97.6)	149.3 (21.7)	6.25	8.25	1123.9 (163)

Conclusions

The uranium-tungsten system shows evidence of age hardening behavior. Solutionizing in the gamma phase, followed by rapid quench into the alpha phase quenches tungsten in solution. Annealing temperatures low in the alpha region give an increase in hardness. Higher in alpha the material overages rapidly. Aging in the beta phase results in a very soft structure.

The majority of the increase in yield strength with the addition of tungsten to uranium is due to precipitation hardening caused by interphase precipitates. Further increases in yield strength are due to composite strengthening, verified by the increase in elastic modulus.

Nucleation and growth of precipitates in the uranium-tungsten system occurs by interphase precipitation at a moving phase boundary during slow cooling. Aging in the alpha region leads to randomization of precipitate location and growth of precipitates. Aging in the beta region followed by slow cooling gives an exaggerated discontinuous lamellar structure which is optically visible. The precipitates are tungsten-rich, the only other possible constituent detectable in STEM analysis being uranium.

Tungsten partially goes into solution in the depleted uranium melt during casting. Impure tungsten powder breaks up extensively along the grain boundaries within the tungsten, while pure tungsten powder breaks up to a much smaller extent. This difference in particle behavior appears to have little effect on the mechanical properties of the material.

The matrix is composed solely of alpha uranium; strengthening is not the result of beta or gamma retained at room temperature.

Wrought material exhibits significant strain hardening as well as composite strengthening due to elongated tungsten particles. Increasing particle L/D ratio results in an increase in modulus with greater deformation of the material.

Further Studies

The effects of powder morphology and impurity levels are currently under study, although no results are reported here. Transmission electron microscopy is being performed on the aged material, for evidence of precipitate formation and coarsening. A study of interphase precipitation kinetics is planned; such a study should prove useful in tailoring material properties through thermomechanical processing. A quench rate sensitivity study, and a simulation of rolling and heat treating are in planning stages awaiting the arrival of a Gleeble. Ternaries are also under investigation for gains in corrosion resistance and as cast ductility.

Endnotes

1. D. Blake, and R.F. Hehemann, "Transformations in Uranium Base Alloys," Physical Metallurgy of Uranium and Uranium Alloys (Columbus, Ohio: Metals and Ceramics Information Center, 1974) 189-218.

2. K.H. Eckelmeyer, Diffusional Transformations, Sterngthening Mechanisms, and Mechanical Properties of Uranium Alloys," Metallurgical Technology of Uranium and Uranium Alloys II (Metals Park, Ohio: American Society for Metals, 1982), 129-202.

3. R.W.K. Honeycombe, Steels: Microstructure and Properties (Metals Park, Ohio: American Society for Metals, 1971).

4. A. Bar-Or, and G. Kimmel, "Phase Transformations in U-Cr Alloys," The Mechanism of Phase Transformations in Crystalline Solids (London: The Institute of Metals, 1969), 325-328.

5. M. Jovanovic, "The Isothermal Groth of Secondary-Phase Particles in a Dilute Uranium Alloy," Journal of Nuclear Materials, 35 (1970), 223-230.

6. Matthew Wm. Lewis, private communication with author, Los Alamos National Laboratory, 31 August, 1989.

7. J.E. Ashton, J.C. Halpin, and P.H. Petit, Primer on Composite Materials (Westport, CT: Technomic Publishing Co., 1969).